ISSN 2616-5880 Vol. 6, Issue 3: 38-45, DOI: 10.25236/AJMC.2025.060304

Efficient Degradation of Sulfadiazine in Wastewater By Co: $Mn_3(PO_4)_2 \cdot 3H_2O$ Composites Activated Peroxymonosulfate

Shikun Song[1], Jingjing Xu[1*]

[1]School of Environmental Science and Engineering, Nanjing University of Information Science & Technology, Nanjing, China
**Corresponding author*

Abstract: *In this study Co:$Mn_3(PO_4)_2 \cdot 3H_2O$(CoMnP-10) catalytic material was prepared by chemical precipitation method, and the morphological structure of the catalyst was optimized by the characterization analysis that Co was uniformly distributed in $Mn_3(PO_4)_2 \cdot 3H_2O$. Experiments results indicated that the CoMnP-10/PMS system demonstrated outstanding degradation capability towards SDZ, and under the optimal conditions (catalyst dosage of 20 mg, PMS concentration of 0.27 mM, and pH at 5.1), 96% removal of pollutants could be achieved within 3 min. The active species involved in the reaction (SO_4^{-}•, •OH, $^1O_2$ and O_2^{-}•) in the CoMnP-10/PMS system were identified by free radical bursting experiments and EPR tests, and the incorporation of Co boosted the electron transfer rate, promoted the Co/Mn dual-metal redox cycling, and thus improved the degradation efficiency of SDZ. According to the above - mentioned research, a reasonable catalytic mechanism for the degradation of SDZ in the CoMnP-10/PMS activation system was proposed.*

Keywords: *Co, $Mn_3(PO_4)_2 \cdot 3H_2O$ Composites, PMS Activation, Sulfadiazine, Degradation Mechanism*

1. Introduction

Sulfonamide antibiotics, as synthetic antimicrobial drugs, have the advantages of ease of use, low price, wide antimicrobial range and high applicability. Among them, SDZ is the most representative sulfonamide antibiotic[1]. However, due to their incomplete utilization, substantial quantities of SDZ are discharged into the environment. Therefore it is important to identify efficient, cost effective and environmentally friendly degradation techniques to remove the contaminants from water.

Non-homogeneous peroxymonosulfate (PMS) activation has shown significant advantages in the field of water remediation, and has achieved breakthroughs in engineering applications in medical wastewater treatment, groundwater remediation and other scenarios. Under the catalysis, PMS generates powerful oxidative reactive species, enabling efficient elimination of refractory contaminants in wastewater. Therefore, the PMS-driven advanced oxidation process is regarded as an innovative technological pathway for the efficient decomposition of difficult-to-degrade pharmaceutical residues and industrial organic pollutants in water bodies.

Manganese is widely available in nature, and elemental manganese (Mn^{2+}, Mn^{3+}, Mn^{4+}) can flexibly participate in the electron transfer reaction with relatively low toxicity, which makes it a reasonable choice for PMS activation, and it is especially excellent in redox catalysis (e.g., Fenton reaction). For example, the transfer of electrons between Mn^{2+}/Mn^{3+} accelerates the PMS activation reaction to degrade difficult-to-remove pollutants in wastewater[2]. $Mn_3(PO_4)_2 \cdot 3H_2O$ can be regulated by synthetic conditions to form nanoparticles, lamellar or porous structures to increase the exposed area of active sites and enhance the catalytic efficiency; it also has the potential of doping modification, and the introduction of transition metals or non-metallic elements can optimize the electronic structure and enhance the catalytic activity and stability, with Multifunctional catalytic applications. With its low cost, high activity, environmental friendliness and structural tunability, manganese phosphate has become an ideal choice to replace precious metal catalysts, especially in the field of environmental pollution control and sustainable energy. It has been confirmed that the modulation of metal oxidation compounds by atomic interfacial engineering can significantly enhance the catalytic performance of catalysts, and Co^{2+} has the best PMS activation performance, therefore, the combination of Co and Mn will be an innovative strategy with research value.

ISSN 2616-5880 Vol. 6, Issue 3: 38-45, DOI: 10.25236/AJMC.2025.060304

In this chapter, Co-doped $Mn_3(PO_4)_2 \cdot 3H_2O$ was prepared by chemical precipitation and used for the degradation of SDZ, an antibiotic in water. The morphology of the catalysts was analyzed by various characterization techniques, demonstrating that Co-doping can improve the catalyst's ability to activate PMS, and suggesting a possible degradation mechanism.

2. Materials and Methods

2.1 Materials

All chemicals and materials are analytically pure unless otherwise stated. The reagents required for this study were:disodium hydrogen sulfate (Na_2HPO_4), magnesium sulfate monohydrate ($MnSO_4 \cdot H_2O$), cobalt chloride hexahydrate ($Cl_2CoH_{12}O_6$), hydrochloric acid (HCl), sodium hydroxide (NaOH), sulfadiazine (SDZ), sodium chloride (NaCl), sodium bisulfate (NaH_2PO_4), sodium sulfate (Na_2SO_4), sodium carbonate (Na_2CO_3), acetonitrile (chromatographic grade), acetic acid (chromatographic grade), peroxymonosulfate (PMS), methanol (MeOH), tertiary butyl alcohol (TBA), benzoquinone (BQ), L-histidine (L-His).

2.2 Catalyst preparation

The preparations in this study were prepared according to the methods of previous studies[3]. 3 mmol Na_2HPO_4 was added to a beaker containing 100 mL of deionized water. Then, $CoCl_2$-$6H_2O$ and $MnSO_4 \cdot H_2O$ with different Co:Mn feed ratios (molar ratios of 1:19, 1:9, and 3:17) were dissolved in the above mixture and stirred continuously at room temperature for 90 min. Next, Co-doped $Mn_3(PO_4)_2 \cdot 3H_2O$ sample. It was named as CoMnP-X and the prepared samples were named as CoMnP-5, CoMnP-10, CoMnP-15 according to the different molar ratios of Co:Mn. In the absence of added $CoCl_2$-$6H_2O$ as described above, the pure $Mn_3(PO_4)_2 \cdot 3H_2O$ was obtained as and was noted as MnP.

2.3 Characterization of catalysts

Crystallographic parameters and phase compositions as well as elemental valence states of the catalysts were analysed by X-ray diffraction (XRD, SmartLab-3KW, Rigaku, Japan) and X-ray photoelectron spectroscopy (XPS, Thermo Scientific K-Alpha, USA). The samples were tested by transmission electron microscopy (TEM, JEOL JEM 2100F, Japan). The pore structure properties of the catalysts were evaluated by testing the BET (Micromeritics ASAP 2460, USA). Samples were tested by electron paramagnetic resonance spectroscopy (EPR, EMXplus-6/1, Bruker, Germany) for capture experiments

3. Results and discussion

3.1 Characterization of MnP and CoMnP

The crystallographic parameters and phase compositions of the catalytic materials were characterized and resolved using XRD. Figure 1a presents the XRD pattern of the catalyst. From the Fig. 1, it is observed that MnP consists of three distinct characteristic peaks 26.78° , 29.60° and 34.66° corresponding to the (111), (202) and (022) crystallographic facets of $Mn_3(PO_4)_2 \cdot 3H_2O$ (JCDS No. 03-0426)[4], respectively, which indicate the successful preparation of MnP. The plots of CoMnP-5, CoMnP-10 and CoMnP-15 and pure MnP are basically the same, and no new diffraction characteristic peaks appeared, which may be due to the fact that no crystalline facets were formed by Co doping in. This is consistent with the previous study that after doping metal Co, the strength of characteristic Co diffraction peaks in the sample XRD is so weak that they are hardly recognizable[5]. In addition, the characteristic peaks of MnP diffraction show a decreasing trend with the continuous increase of Co content, which indicates that the lattice disorder of the samples has increased and the crystallinity has decreased.

TEM and HRTEM analyses of MnP and CoMnP-10 samples were carried out to characterize the crystal structure of the catalysts. In Fig. 1b, it can be observed that MnP shows elongated needle-like or fibrous particles. The TEM characterization results of CoMnP-10 samples are shown in Fig. 1c, after the addition of Co, the morphology changes to a more lamellar structure, and the particles seem to be

ISSN 2616-5880 Vol. 6, Issue 3: 38-45, DOI: 10.25236/AJMC.2025.060304

more tightly stacked with each other. CoMnP-10 This change in morphology and size is undoubtedly beneficial for the catalytic reaction, and usually has a larger specific surface area provides a richer set of reaction sites for the reaction process. which can provide more active sites and facilitate electron transport in the catalytic reaction. As revealed by the HRTEM (Fig. 1d) results, the decrease in the crystallinity of the CoMnP-10 samples resulted from the doping of Co., and short-range ordered lattice fringes can be seen only locall. In Fig. 1d, the presence of j clearer lattice stripes in the sample has a lattice spacing accurately determined to be 0.2470 nm; this spacing is confirmed by the crystal surface index analysis to be in high agreement with the standard value of (022) crystal surface of CoMnP-10 material. Thus, the TEM results further demonstrate the successful preparation of the composite.

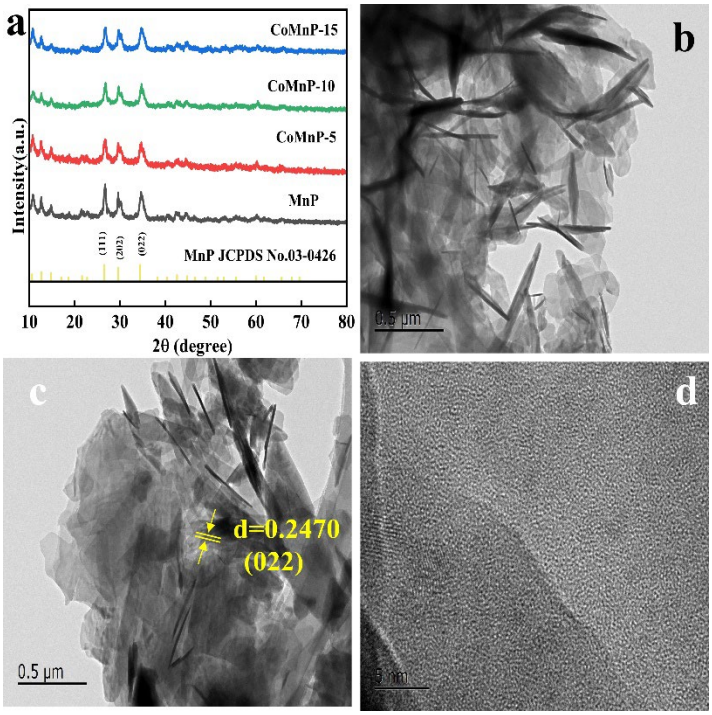

Fig.1 (a)X-ray diffraction spectrum of CoMnP and MnP composite samples(b) MnP TEM image, (c) CoMnP-10 TEM image and (d) CoMnP-10 HRTEM image

The pore structure and specific surface area of MnP and CoMnP-10 were characterized using N_2 adsorption and desorption physical experiments. Both MnP and CoMnP-10 show typical type IV isotherms (Fig. 2a-b), both conforming to H3 hysteresis loops, indicating the presence of mesoporous structure or irregular pores in the material[6]. As can be seen from Fig. 2a, the pore size of CoMnP-10 is mainly distributed in the 0-50 nm interval, and its peak value is about 0-5 nm. According to the BJH calculation method (Table 1), the BET specific surface area(SSA) of CoMnP-10 was measured to be 24.9422 m^2/g, which exhibits a minor increase compared to that of MnP (22.7521 m^2/g), implying that it has more reactive surfaces, which is important for reactivity and adsorption of reactants in the catalytic reaction, and the smaller pore sizes of CoMnP-10 may contain more micropores or small pores, thus the increased SSA of the material exposes more active sites, thus accelerating, the reaction rate of CoMnP-10.

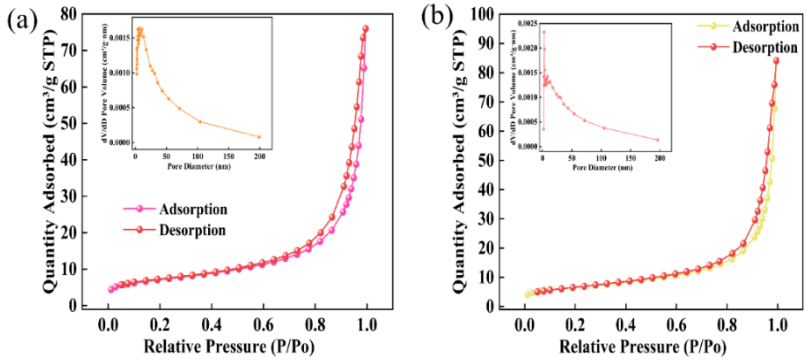

Fig.2 N2 adsorption-desorption isotherms for (a) CoMnP-10 and (b) MnP

ISSN 2616-5880 Vol. 6, Issue 3: 38-45, DOI: 10.25236/AJMC.2025.060304

Table 1 BET parameters of CoMnP-10 and MnP

samples	BET surface area (m^2/g)	Average pore size (nm)	pore volume (cm^3/g)
CoMnP-10	24.9422	18.8471	0.002163
MnP	22.7521	22.5107	0.001661

The two catalysts, CoMnP-10 and MnP, were subjected to XPS tests so as to further analyze the elemental species and content of the materials as well as the valence distribution characteristics. The CoMnP-10 complex in Fig. 3a shows characteristic peaks of Co 2p, W 4f, Ce 3d and O 1s, whereas MnP contains the elements Mn, P, and O, which proves that the XRD does not contain impurity elements and confirms the successful doping of Co metal in the CoMnP-10 composites. The Co 2p spectra is presented in Fig. 3b, where the Co $2p_{3/2}$ and Co $2p_{1/2}$ spectral features display binding energies of 781.6 eV and 797.6 eV, respectively.[7]. In the Mn 2p spectra (Fig. 3c), the signal peaks located at 641.2 eV and 642.5 eV correspond to Mn $2p_{1/2}$ and Mn $2p_{3/2}$, proving that Mn^{2+} and Mn^{3+} are contained in the CoMnP-10 material[8], and one of the signal peaks at 646.2 eV corresponds to the Mn^{2+} satellite peak of Mn $2p_{3/2}$[9, 10]. Fig 3d shows the high-resolution spectra of O 1s, which is deconvoluted into four signal peaks at 528.2, 531.2, 532.5 and 533.7 eV. These peaks are respectively assigned to O_L, -OH, PO_4^{3-}, and adsorbed H_2O[3, 11], where the -OH content is very high, which is favorable for the free radical[12, 13] generation.

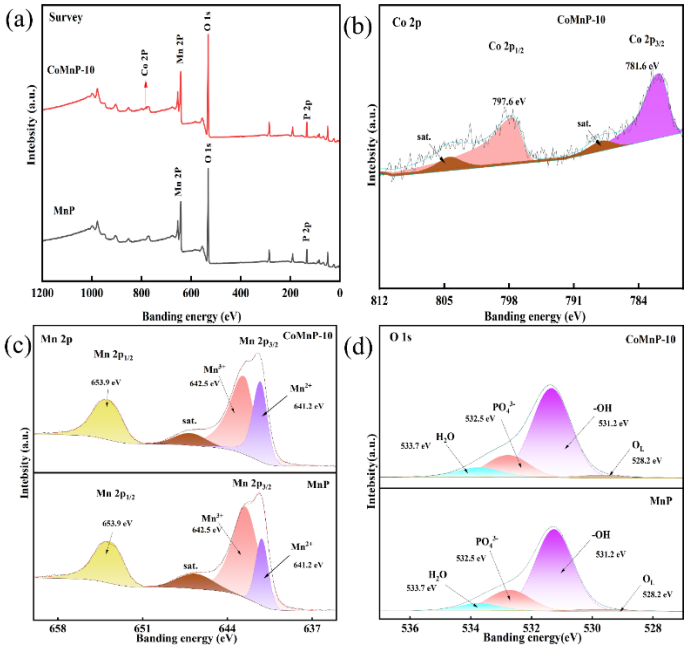

Fig.3 (a) XPS full spectra of CoMnP-10 and MnP; (b) Co 2p; (c) Mn 2p; (d) O 1s

3.2 Performance of activation degradation of SDZ

In this study, SDZ was used as a probe pollutant, and degradation experiments were conducted under dark conditions in order to exclude photochemical interferences. The catalytic performance of MnP, CoMnP-5, CoMnP-10 and CoMnP-15 was comprehensively evaluated to achieve the removal of SDZ by activating PMS. In the absence of PMS injection (Fig. 4a), the removal of SDZ by pure MnP was only about 1% in 20 min, while only CoMnP-10 showed the best removal effect among the doped samples, but only 4%, so MnP as well as the doped samples have no ability to remove SDZ by themselves. Fig. 4b shows the comparison graph of PMS addition, and it can be found that under the condition of only adding PMS without catalyst, the effect of PMS itself on SDZ removal is only 6%, therefore, single component PMS could not oxidize SDZ effectively. Under the same conditions, the MnP/PMS system did not exhibit desirable degradation properties, and the degradation efficiency of the MnP/PMS system for SDZ at 20 min was only 39%. In the samples of Co-doped MnP (CoMnP-5, CoMnP-10, and CoMnP-15), the activated PMS performance of the catalysts was gradually enhanced with the increase of Co-doping amount, which demonstrated the importance and effectiveness of Co as a typical active site, and even the activated PMS performance of the sample with the smallest percentage of Co doping (CoMnP-5) was higher than the MnP activation performance, which degraded

ISSN 2616-5880 Vol. 6, Issue 3: 38-45, DOI: 10.25236/AJMC.2025.060304

SDZ up to 87%. The CoMnP-10/PMS system The degradation performance of SDZ reached 98% at 5 min, which was the best degradation effect. Comparing the two samples of CoMnP-10 and CoMnP-15, it can be found that the degradation effect of SDZ at 20 min is very close, so the catalytic activation performance of CoMnP-10 and CoMnP-15 was compared at 5 min, as shown in Fig. 5c. Within the initial 0.5-minute interval, the degradation efficacy of CoMnP-15 exceeded that of CoMnP-10., but as the reaction time continued, the removal of SDZ by CoMnP-15 gradually became slower, and after 0.5 min, the catalytic activation performance of CoMnP-10 was higher than that of CoMnP-15, The catalytic activation performance of CoMnP-10 was higher than that of CoMnP-15, and the degradation of SDZ by the CoMnP-10/PMS system reached 96% at 3 min. In light of the preceding experimental results, CoMnP-10 was the best sample in terms of economic cost and Co leaching.

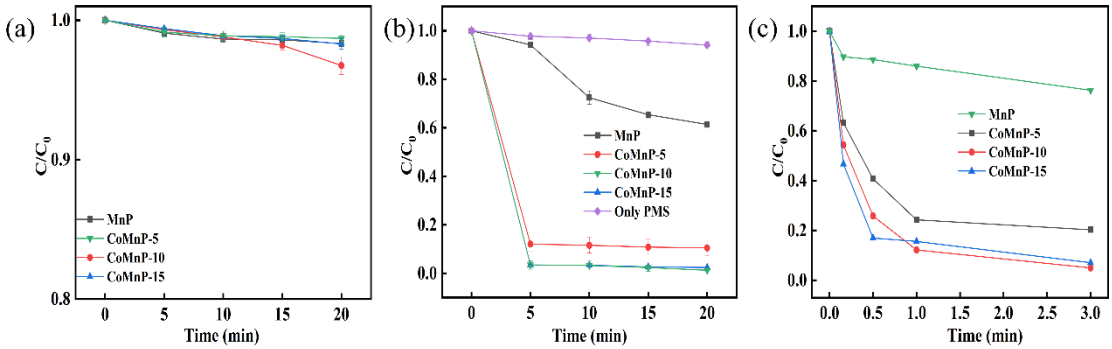

Fig.4 (a) Degradation curves for each catalyst (without PMS); (b-c) SDZ degradation curves by PMS activated by different catalysts

3.3 Identification and reaction mechanisms of free radicals

Selective quenching experiments were performed by introducing specific reactive oxygen species inhibitors to analyze the major reactive oxygen species in the CoMnP-10/PMS system[14, 15]. Methanol (MeOH) was employed to inhibit the contribution of •OH and SO_4^{-}• simultaneously, and tert-Butanol (TBA) was utilized to selectively quench •OH (whereas the quenching ability of SO_4^{-}• was negligible), and p-benzoquinone (BQ) was added to eliminate O_2^{-}• and histidine (L-His, which removes $^1O_2$ by a dual mechanism of physical quenching and chemical binding), respectively [16]. The quenching experiment results, as presented in Fig. 5a, when MeOH was added to the CoMnP-10/PMS system, the degradation of SDZ appeared to be greatly inhibited, with a degradation efficiency of only 12.7%, which indicated that SO_4^{-}• and •OH were the primary reactive species responsible in the SDZ removal process. However, when TBA was added, a weak inhibition of degradation of SDZ was observed, a phenomenon that suggests that •OH has a limited role in the degradation of SDZ, while SO_4^{-}• is the main active species. Whereas, the introduction of BQ and L-His into the CoMnP-10/PMS system, a significant inhibition of both SDZ degradation efficiencies could be observed, with degradation efficiencies of 75% and 81%, respectively, which suggests that O_2^{-}• and $^1O_2$ also contribute significantly to the removal of SDZ.

To resolve the controversy about major reactive oxygen species (ROS), DMPO and TEMP was used as a ROS trapping agent, and the ROS species in the reaction system were comprehensively analysed by EPR technique, enables the detection and evaluation of free radicals. The experimental results in Fig. 5b show that, in the CoMnP-10/PMS/DMPO test system, the presence of only 1:2:1:2:2:1:2:1 seven-fold signal peaks was detected, which is the characteristic peak of DMPO-X generated by oxidation of DMPO. This is due to the fact that there is too much oxidizing in the system, resulting in the trapping agent DMPO being oxidized to open the ring, there is no way to act as a trapping agent as it was originally intended to do, and the appearance of DMPO-X may be attributed to the aggressive oxidation of DMPO by successive hydroxylation reactions or other free radicals[17, 18]. There is no detection of DMPO-SO_4^{-}• in the EPR pattern and the DMPO-•OH signal peaks, while the characteristic peak of DMPO-X appeared, which does not indicate that SO_4^{-}• and •OH[19] are not present in the system. Precisely indicating that DMPO is oxidized at a much faster rate than DMPO as a spin trapping agent, weak signal peaks were also observed for DMPO-O_2^{-}• and TEMP-$^1O_2$. The results of the bursting experiments were confirmed.

ISSN 2616-5880 Vol. 6, Issue 3: 38-45, DOI: 10.25236/AJMC.2025.060304

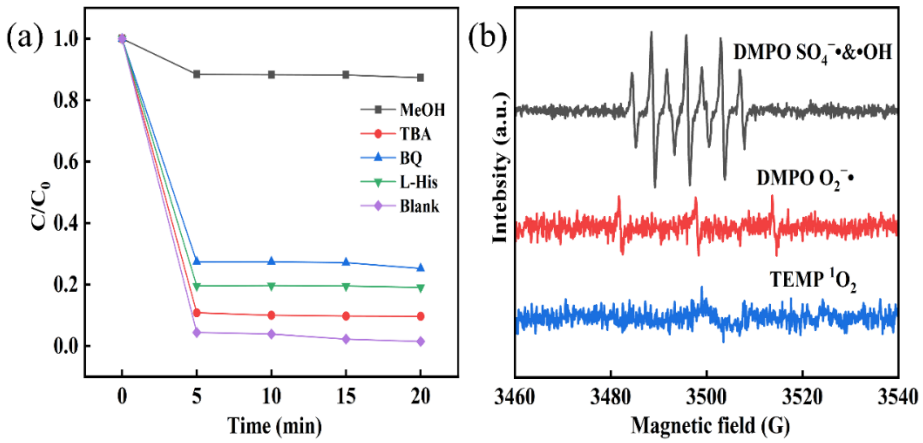

Fig.5 (a) Free radical burst experiment of CoMnP-10/PMS; (b) EPR spectra of DMPO and TEMP as spin traps (reaction conditions: catalyst = 20 mg, SDZ = 5 mg/L, PMS = 0.27 mM, pH = 5.1, temperature = 25℃)

The mechanism of activation of PMS for SDZ removal by CoMnP-10 catalyst was elucidated through identification of active species and EPR analysis, combined with the characterization and analytical results from this study. A lot of metal ions (Co^{2+}/Mn^{2+}) in the composite material CoMnP-10, which can trigger the conversion of HSO_5^- to SO_4^-•, as in Eq. (1), (2); after that, the generated SO_4^-• reacts with H_2O to form •OH (Eq.3), after which Co^{3+}/Mn^{3+} is reduced by HSO_5^- to produce SO_5^-• and Co^{2+}/Mn^{2+}(Eq. 4-5)[20], which results in the formation of Co^{2+}/Co^{3+} and Mn^{2+} /Mn^{3+} redox cycles. Due to the higher standard reduction potential of Co^{3+}/Co^{2+} (E_0=1.81 V) than that of Mn^{3+}/Mn^{2+}(E_0=1.51 V)[21, 22], which this potential difference property facilitates rapid electron transfer and increases the rate of reaction (Eq. 6). On the other hand, SO_5^-• reacts with H_2O to form O_2^-•[23] (Eq. 7), after which it is further converted to $^1O_2$(Eq. 8). Briefly, three radical pathways (SO_4^-•, •OH, and O_2^-•) together with one non-radical pathway $^1O_2$ degraded SDZ in the CoMnP-10/PMS system.The degradation mechanism diagram is shown in Figure 6.

$$Co^{2+} + HSO_5^- \rightarrow Co^{3+} + SO_4^- \bullet + OH^- \quad (1)$$

$$Mn^{2+} + HSO_5^- \rightarrow Mn^{3+} + SO_4^- \bullet + OH^- \quad (2)$$

$$SO_4^- \bullet + H_2O \rightarrow \bullet OH + SO_4^{2-} + H^+ \quad (3)$$

$$Co^{3+} + HSO_5^- \rightarrow Co^{2+} + SO_5^- \bullet + H^+ \quad (4)$$

$$Mn^{3+} + HSO_5^- \rightarrow Mn^{2+} + SO_5^- \bullet + H^+ \quad (5)$$

$$Co^{3+} + Mn^{2+} \rightarrow Co^{2+} + Mn^{3+} \quad \Delta E=0.30V \quad (6)$$

$$SO_5^- \bullet + H_2O \rightarrow SO_4^{2-} + O_2^- \bullet + 2H^+ \quad (7)$$

$$O_2^- \bullet + \bullet OH \rightarrow {}^1O_2 + OH^- \quad (8)$$

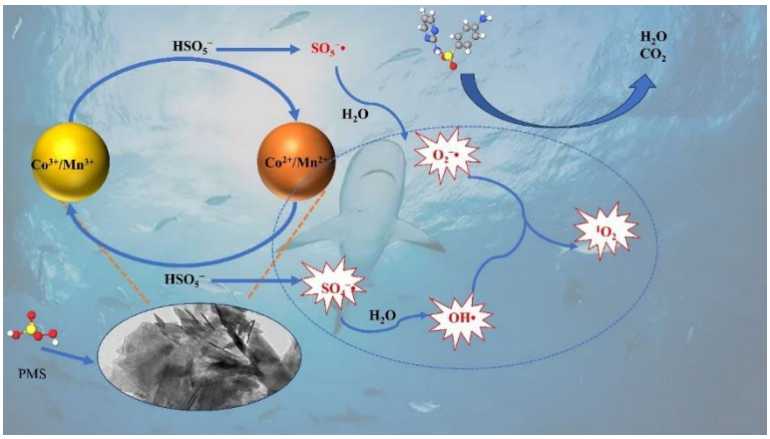

Fig.6 Mechanism of SDZ degradation by CoMnP-10/PMS

ISSN 2616-5880 Vol. 6, Issue 3: 38-45, DOI: 10.25236/AJMC.2025.060304

4. Conclusion

In this study, Co-doped $Mn_3(PO_4)_2 \cdot 3H_2O$ catalytic materials were prepared by chemical precipitation method, and antibiotic SDZ was selected as the degradation target, and the performance of Co: $Mn_3(PO_4)_2 \cdot 3H_2O$ (CoMnP-10) catalytic materials was evaluated for activation of PMS. The results of XRD, TEM, and XPS showed that Co was successfully doped into $Mn_3(PO_4)_2 \cdot 3H_2O$. The metal Co was uniformly distributed inside $Mn_3(PO_4)_2 \cdot 3H_2O$. From the analysis of the BET results, CoMnP-10 showed an increase in the specific surface area, which was conducive to adsorb the PMS on the surface for reaction. The composite CoMnP-10 had the best performance in activating PMS, at the optimal catalytic environment, 96% removal of SDZ was achieved in 3 min. Free radical burst experiments and EPR tests finalized that the ROS in the degradation process in the CoMnP-10/PMS system were SO_4^{-}•, •OH, $^1O_2$ and O_2^{-}•. The CoMnP-10 composite catalysts showed good performance and excellent adaptability in activating the PMS for the degradation of organic pollutants in water.

References

[1] F. Chen, F. Yang, H. Liu, S. Che, G. Zhang, C. Xu, Y. Li, One-pot preparation of surface vulcanization Co-Fe bimetallic aerogel for efficient sulfadiazine degradation, Chemical Engineering Journal, 430 (2022) 132904.

[2] X. Zhai, W. Yang, M. Li, G. Lv, J. Liu, X. Zhang, Noncovalent hybrid of $CoMn_2O_4$ spinel nanocrystals and poly (diallyldimethylammonium chloride) functionalized carbon nanotubes as efficient electrocatalysts for oxygen reduction reaction, Carbon, 65 (2013) 277-286.

[3] Y. Li, Z.-R. Jiang, X. Yang, Y. Lan, J. Guo, Structure of a novel Co-based heterogeneous catalyst via $Mn_3(PO_4)_2$ as a carrier to efficiently activate peroxymonosulfate for improving degradation of sulfonamides, Chemosphere, 325 (2023) 138337.

[4] J. Yu, W. Qiu, H. Xu, X. Lu, J. Ma, D. Lu, Highly-efficient and stable $MgCo_2O_4$ spinel for bisphenol a removal by activating peroxymonosulfate via radical and non-radical pathways, Chemical Engineering Journal, 421 (2021) 129498.

[5] Y. Liu, W. Guo, H. Guo, X. Ren, Q. Xu, Cu (II)-doped V_2O_5 mediated persulfate activation for heterogeneous catalytic degradation of benzotriazole in aqueous solution, Separation and Purification Technology, 230 (2020) 115848.

[6] Y. Xie, H. Sun, L. Luo, T. Peng, J. Tian, Preparation of high diameter-thickness ratio thin-layer phlogopite-vermiculite nano-functional material by liquid phase exfoliation, Applied Clay Science, 191 (2020) 105612.

[7] W. Zhu, X. Tang, F. Gao, H. Yi, R. Zhang, J. Wang, C. Yang, S. Ni, The effect of non-selective oxidation on the $Mn_2Co_1O_x$ catalysts for NH3-SCR: Positive and non-positive, Chemical Engineering Journal, 385 (2020) 123797.

[8] J. Li, J. Fang, L. Gao, J. Zhang, X. Ruan, A. Xu, X. Li, Graphitic carbon nitride induced activity enhancement of OMS-2 catalyst for pollutants degradation with peroxymonosulfate, Applied Surface Science, 402 (2017) 352-359.

[9] L. Dai, Y. Wang, L. Sun, Y. Ding, Y. Yao, L. Yao, N.E. Drewett, W. Zhang, J. Tang, W.J.A.S. Zheng, Jahn–Teller Distortion Induced Mn^{2+}-Rich Cathode Enables Optimal Flexible Aqueous High-Voltage Zn-Mn Batteries, Advanced Science, 8 (2021) 2004995.

[10] J. Fan, H. Qin, S. Jiang, Mn-doped g-C_3N_4 composite to activate peroxymonosulfate for acetaminophen degradation: The role of superoxide anion and singlet oxygen, Chemical Engineering Journal, 359 (2019) 723-732.

[11] Z.-R. Jiang, Y. Li, Y.-X. Zhou, X. Liu, C. Wang, Y. Lan, Y. Li, Co_3O_4-MnO_2 nanoparticles moored on biochar as a catalyst for activation of peroxymonosulfate to efficiently degrade sulfonamide antibiotics, Separation and Purification Technology, 281 (2022) 119935.

[12] L. Chen, S. Yang, X. Zuo, Y. Huang, T. Cai, D. Ding, Biochar modification significantly promotes the activity of Co_3O_4 towards heterogeneous activation of peroxymonosulfate, Chemical Engineering Journal, 354 (2018) 856-865.

[13] Y. Lü, W. Zhan, Y. He, Y. Wang, X. Kong, Q. Kuang, Z. Xie, L. Zheng, MOF-Templated Synthesis of Porous Co_3O_4 Concave Nanocubes with High Specific Surface Area and Their Gas Sensing Properties, ACS Applied Materials & Interfaces, 6 (2014) 4186-4195.

[14] H. Fu, S. Ma, P. Zhao, S. Xu, S. Zhan, Activation of peroxymonosulfate by graphitized hierarchical porous biochar and $MnFe_2O_4$ magnetic nanoarchitecture for organic pollutants degradation: Structure dependence and mechanism, Chemical Engineering Journal, 360 (2019) 157-170.

[15] Y. Zhao, M. Song, Q. Cao, P. Sun, Y. Chen, F. Meng, The superoxide radicals' production via

ISSN 2616-5880 Vol. 6, Issue 3: 38-45, DOI: 10.25236/AJMC.2025.060304

persulfate activated with $CuFe_2O_4$@Biochar composites to promote the redox pairs cycling for efficient degradation of o-nitrochlorobenzene in soil, Journal of Hazardous Materials, 400 (2020) 122887.
[16] X. Sun, D. Xu, P. Dai, X. Liu, F. Tan, Q. Guo, Efficient degradation of methyl orange in water via both radical and non-radical pathways using Fe-Co bimetal-doped MCM-41 as peroxymonosulfate activator, Chemical Engineering Journal, 402 (2020) 125881.
[17] M. Huang, Y.-S. Li, C.-Q. Zhang, C. Cui, Q.-Q. Huang, M. Li, Z. Qiang, T. Zhou, X. Wu, H.-Q. Yu, Facilely tuning the intrinsic catalytic sites of the spinel oxide for peroxymonosulfate activation: From fundamental investigation to pilot-scale demonstration, Proceedings of the National Academy of Sciences of the United States of America, 119 (2022) e2202682119.
[18] J. Huang, Y. Dai, K. Singewald, C.-C. Liu, S. Saxena, H. Zhang, Effects of MnO_2 of different structures on activation of peroxymonosulfate for bisphenol A degradation under acidic conditions, Chemical Engineering Journal, 370 (2019) 906-915.
[19] G. Cai, Y. Tian, L. Li, W. Zhang, R. Huang, J. Zhang, Q. Wang, H. Xu, Y. Zhang, Sulfite activation of Fe-Mn bimetallic oxides for rapid oxidative removal of As(III) in water: Involvement of active Mn(III), Chemical Engineering Journal, 479 (2024) 147539.
[20] Y. Zhang, J.-B. Huo, J.-C.E. Yang, M.-L. Fu, Facile fabrication of elastic CoO@graphene aerogel for recycled degradation of chloramphenicol, Materials Letters, 240 (2019) 88-91.
[21] C.-X. Li, C.-B. Chen, J.-Y. Lu, S. Cui, J. Li, H.-Q. Liu, W.-W. Li, F. Zhang, Metal organic framework-derived $CoMn_2O_4$ catalyst for heterogeneous activation of peroxymonosulfate and sulfanilamide degradation, Chemical Engineering Journal, 337 (2018) 101-109.
[22] S. Kang, J. Hwang, $CoMn_2O_4$ embedded hollow activated carbon nanofibers as a novel peroxymonosulfate activator, Chemical Engineering Journal, 406 (2021) 127158.
[23] G. Zhang, Y. Wang, M. Chen, J. Xu, L. Wang, ZIF-67-derived carbon@Co_3S_4/$CoSO_4$/MnO polyhedron to activate peroxymonosulfate for degrading levofloxacin: Synergistic effect and mechanism, Chemical Engineering Journal, 451 (2023) 138976.